JARO 14: 611–622 (2013)
DOI: 10.1007/s10162-013-0407-y

JARO
Journal of the Association for Research in Otolaryngology

Research Article

An Analysis of the Acoustic Input Impedance of the Ear

Robert H. Withnell[1,2,3] and Lauren E. Gowdy[1]

[1]*Department of Speech and Hearing Sciences, Indiana University, Bloomington, IN 47405, USA*
[2]*Neuroscience Program, Indiana University, Bloomington, IN 47405, USA*
[3]*Department of Physics, Indiana University, Bloomington, IN 47405, USA*

Received: 8 October 2012; Accepted: 4 July 2013; Online publication: 6 August 2013

ABSTRACT

Ear canal acoustics was examined using a one-dimensional lossy transmission line with a distributed load impedance to model the ear. The acoustic input impedance of the ear was derived from sound pressure measurements in the ear canal of healthy human ears. A nonlinear least squares fit of the model to data generated estimates for ear canal radius, ear canal length, and quantified the resistance that would produce transmission losses. Derivation of ear canal radius has application to quantifying the impedance mismatch at the eardrum between the ear canal and the middle ear. The length of the ear canal was found, in general, to be longer than the length derived from the one-quarter wavelength standing wave frequency, consistent with the middle ear being mass-controlled at the standing wave frequency. Viscothermal losses in the ear canal, in some cases, may exceed that attributable to a smooth rigid wall. Resistance in the middle ear was found to contribute significantly to the total resistance. In effect, this analysis "reverse engineers" physical parameters of the ear from sound pressure measurements in the ear canal.

Keywords: ear canal acoustics, input impedance

INTRODUCTION

The acoustic input impedance of the ear quantifies how the ear receives sound. The ear canal, the middle ear, and the cochlea all contribute to this acoustic input impedance. Over the frequency region that sound propagates predominantly as plane waves, the ear canal is thought to be reasonably described by a uniform cylinder or tube with rigid walls (Stinson 1985). The middle ear and cochlea act as a distributed load impedance, with sound energy being transferred to the cochlea in a frequency-dependent manner.

Previous studies of the acoustic input impedance of the ear include lumped element models of the human middle ear (e.g., Kringlebotn 1988; Moller 1961; Zwislocki 1962), experimental studies of the middle ear of human temporal bones (e.g., O'Connor and Puria 2008; Voss et al. 2000), experimental studies of human ears (e.g., Farmer-Fedor and Rabbitt 2002; Kringlebotn 1994; Margolis et al. 1999; Moller 1965; Rabinowitz 1981; Voss and Allen 1994), and models and experimental studies of animal ears (e.g., Huang et al 2000; Lynch et al. 1994; Parent and Allen 2007). Prior to 1981, experimental studies of the acoustic input impedance of the ear in humans were limited to about 1.5 kHz, the ear canal treated as an acoustic compliance (Rabinowitz 1981). The ear canal, modeled as a one-dimensional transmission line, extends the upper frequency limit to where sound deviates from propagating predominantly as plane waves. Kringlebotn (1988) modeled the human ear canal as a lossy transmission line terminated by a load impedance, the middle ear, and the cochlea. His middle ear model was similar to that of Zwislocki (1962), incorporating the middle ear cavities, eardrum and ossicles, cochlea, and shunts for energy reflected from the middle ear and not transferred to the cochlea. Kringlebotn (1988) obtained values for his model elements from published studies for element values that were fixed in the model and used a method of least squares to fit the model to the data average obtained from human temporal bones for model

Correspondence to: Robert H. Withnell · Department of Physics · Indiana University · Bloomington, IN 47405, USA. email: rwithnel@indiana.edu

elements that were free to vary. O'Connor and Puria (2008) examined transfer functions of the middle ear using a model that did not include the ear canal or cavities of the middle ear, focusing on the function of the transmission of sound from the eardrum to the cochlea via the ossicular chain. A modified version of Zwislocki's model of the middle ear was used with the eardrum incorporated as a delay line. As for Kringlebotn (1988), parameters for the model were obtained by fitting the model to data from human temporal bones. O'Connor and Puria (2008) modeled the cochlear input impedance as resistive, consistent with Zwislocki's suggestion that the cochlear input impedance is predominantly resistive, although there is a compliant reactance element (Aibara et al. 2001). Kringlebotn (1988) included compliant reactance and mass reactance terms for the cochlea in his model.

Using transmission line theory, this study examined the respective contributions of the ear canal, middle ear, and cochlea, to the acoustic input impedance of the ear. In contrast to most previous studies, the model was fit to individual data rather than the data average, and for healthy human ears. The ear canal was modeled as a one-dimensional lossy transmission line, with a more exact treatment of viscothermal losses than that provided by Kringlebotn (1988). The middle ear model incorporated the middle ear cavities, eardrum and ossicles, and cochlea with the eardrum and ossicles represented by a bank of resonant filters rather than the single resonant filter and shunts of Zwislocki/Kringlebotn. For the model fit to data, using a nonlinear least squares fit algorithm, only ear canal radius, ear canal length, and resistance parameters (losses in the ear canal, middle ear, and cochlea) were free to vary. Compliant and mass reactance terms were fixed in the fitting algorithm. Compliant reactance terms were based on published data, altered to accommodate individual data. Mass reactance terms were drawn from published data.

METHODS

Subjects and Data Collection

Sound pressure measurements were made in one ear of subjects aged 18–30 years, the location of measurement being near the isthmus. Subject inclusion required the ear canal resonance to be below 6 kHz. Data is presented from six subjects, four female and two male. The method for data collection has been described previously (see Withnell et al. 2009). Briefly, signal generation and data acquisition was computer-controlled using the Mimosa HearID system with version R4 software module (www.mimosaacoustics.com). Sound pressure was measured in the ear canal by a device that housed two speakers and one microphone (ER10CP; www.etymoticresearch.com) with probe tubes connecting the transducers to the ear via a foam eartip (ER14A/B). The foam eartip compressed for insertion in the ear canal, expansion of the foam eartip providing an acoustic seal. The sound stimulus was a rising chirp with a bandwidth of 210–6,000 Hz. The microphone signal was amplified 40 dB and digitized at a rate of 48 kHz. Microphone sensitivity was 50 mV/Pa; sound pressure measurements were corrected in software for the frequency response of the microphone. The Thevenin equivalent acoustic impedance (Z_s) and pressure (P_s) of the ER10CP was determined using four cavities of known acoustic impedance and solving this overdetermined system (Voss and Allen 1994). The acoustic input impedance for each ear (the data) was then calculated using the equation:

$$Z_{\text{in}} = Z_s\left(\frac{P_{\text{mic}}}{P_s - P_{\text{mic}}}\right), \tag{1}$$

where Z_s is the source acoustic impedance, P_s is the source acoustic pressure, and P_{mic} is the sound pressure measured at the microphone in the ear canal. This study was completed with the approval of the Indiana University Institutional Review Board.

Modeling and Data Analysis

The ear was modeled as a one-dimensional lossy transmission line terminated by a distributed load impedance (a non-rigid termination), applicable to plane wave sound propagation. The ear canal was represented by a lossy transmission line. The middle ear and cochlea, the load impedance, was represented by a circuit that incorporates: (1) the middle ear cavities using the circuit of Kringlebotn (1988); (2) the eardrum and ossicles using a bank of five simple harmonic oscillators, or simple mass–spring systems (each tuned to a different frequency), arranged in parallel. Five oscillators were chosen to represent the eardrum and ossicles based on the maximum number of resonances suggested in the data; and (3) the cochlea as an *RC* circuit. Figure 1 shows the circuit diagram for this model.

The acoustic input impedance for the model is given by Kringlebotn (1988): [1]

$$Z_e = Z_0\frac{Z_{\text{me}} + iZ_0\tan(-i\Gamma l)}{Z_0 + iZ_{\text{me}}\tan(-i\Gamma l)}, \tag{2}$$

[1] Equation 2 was derived by combining Eqs. 18, 17, and 12 from Kringlebotn, with a modicum of algebra, and using a trigonometric identity for the tangent function in terms of e.

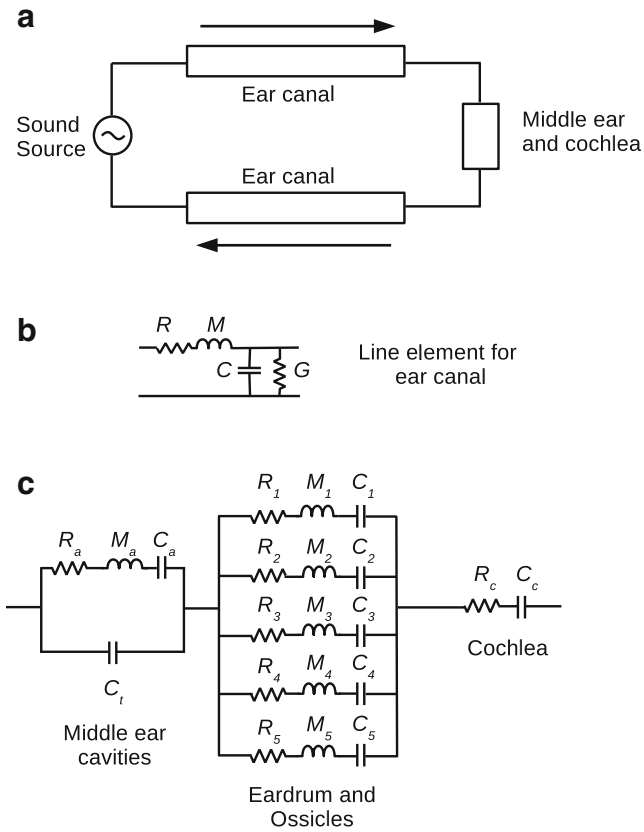

FIG. 1. The circuit diagram for the model of the ear used in this study. The ear was modeled as a one-dimensional lossy transmission line (ear canal) terminated by a distributed load impedance, the middle ear and cochlea. This model is shown in **a**, with the two paths for the transmission line, a wave going in and a wave coming out, terminated by the load impedance. The line element for the transmission line is shown in **b**, consisting of a series impedance and a shunt admittance. The series impedance consists of resistance (*R*) and mass (*M*), the shunt admittance consists of conductance (*G*), and compliance (*C*). The resistance corresponds to viscous losses, the conductance to thermal losses, at the wall of the ear canal (Benade 1968). The load impedance, the middle ear and cochlea, is shown in **c**. The middle ear model incorporates the middle ear cavities (from Kringlebotn 1988), eardrum and ossicles, and cochlea. The eardrum and ossicles are represented by a bank of resonant filters, and the cochlea is represented by an RC circuit.

where Z_{me} is the input impedance of the middle ear and cochlea, l is the physical length of the ear canal, and Z_0 is the characteristic impedance of the ear canal. Z_0 is given by:

$$Z_0 = \frac{R + iwM}{\Gamma}, \tag{3}$$

with Γ being the propagation term,

$$\Gamma = \alpha + i\beta = \sqrt{(R + iwM)(G + iwC)}, \tag{4}$$

where α describes the attenuation of the sound due to resistive losses and β describes the propagation properties of the sound in the ear canal.

The radius of the ear canal is given by:

$$r = a\Upsilon_{LF}, \tag{5}$$

where a is the parameter in the nonlinear fitting of the model to the data that sets the final value of the radius, and Υ_{LF} is the initial value for the radius. The initial value for the radius was the acoustic radius at low frequencies, given by:

$$\Upsilon_{LF} = \frac{1}{n}\sum\left(\frac{\cot(2\pi f_i L/c)\rho c}{\pi|Z_{LF}|}\right)^{0.5}, \tag{6}$$

where L is the acoustic length at the standing wave frequency (SWF), c is the velocity of sound, ρ is the density of air, Z_{LF} is the acoustic input impedance of the ear at low frequencies, f_i is the frequency, and n is the number of frequencies. f_i ranged from 210 to 490 Hz.

The length of the ear canal is given by:

$$l = bL, \tag{7}$$

where b is the parameter in the nonlinear fitting of the model to the data that sets the final value of the length and L is the acoustic length at the SWF.

The elements of the lossy transmission line (the ear canal), see Figure 1, are given by (Benade 1968):

$$R = -\frac{w\rho}{\pi r^2}\left[\frac{F_v sin\theta_v}{D^2}\right], \tag{8}$$

$$M = \frac{\rho}{\pi r^2}\left[\frac{1-F_v cos\theta_v}{D^2}\right], \tag{9}$$

$$G = -\frac{w\pi r^2}{\rho c^2}[(\delta-1)F_t sin\theta_t], \tag{10}$$

and

$$C = \frac{\pi r^2}{\rho c^2}[1+(\delta-1)F_t sin\theta_t], \tag{11}$$

where R is the series (acoustical) resistance per unit length of the transmission line (viscous losses), M is the series inertance per unit length, G is the shunt conductance per unit length (thermal losses), C is the shunt compliance per unit length, and

$$F_v e^{i\theta_v} = \frac{2}{\varphi_v\sqrt{-i}}\frac{J_1[\varphi_v\sqrt{-i}]}{J_0[\varphi_v\sqrt{-i}]}, \tag{12}$$

$$F_t e^{i\theta_t} = \frac{2}{\varphi_t\sqrt{-i}}\frac{J_1[\varphi_t\sqrt{-i}]}{J_0[\varphi_t\sqrt{-i}]}, \tag{13}$$

and

$$D^2 = (1-F_v cos\theta_v)^2 + (F_v sin\theta_v)^2, \tag{14}$$

where w is angular frequency, r is the radius, c is the velocity of sound, ρ is the density of air, and δ is the ratio of specific heats of air. J_0 is the Bessel function of order 0 and J_1 is the Bessel function of order 1. φ is the ratio of the radius of the ear canal to the boundary layer (with subscript v for viscous and t for thermal).

For longitudinal wave propagation in a cylinder or tube with a smooth, rigid wall, the ratios of the radius of the tube to the viscous and thermal boundary layers are given by Benade (1968):

$$\varphi_v = r\sqrt{\frac{w\rho}{\eta}}, \tag{15}$$

and

$$\varphi_t = r\sqrt{\frac{w\rho C_p}{K_t}}, \tag{16}$$

where w is angular frequency, r is the radius, ρ is the density of air, η is the viscosity of air, C_p is the specific heat of air at constant pressure, and K_t is the thermal conductivity. The theory for sound propagation in a tube, incorporating viscous and thermal losses, was provided by Kirchhoff in 1868 (Henry 1931; Weston 1953; Shields et al. 1965).

A wall surface that is not smooth causes disagreement between theory and experiment (Weston 1953). Indeed, Kirchhoff observed that "if the smooth surface of the tube is made rough, the effect of viscosity as well as that of heat conduction must increase" (Henry 1931). In effect, with respect to Kirchhoff's theory, wall surface roughness decreases the effective diameter of the tube (Kaye and Sherratt 1933), which is the same as saying it increases the size of the boundary layer from that predicted by Kirchhoff.

The ear canal wall is neither smooth, nor rigid, and so the boundary layer would be expected to be different from that of a smooth, rigid wall. The more general expressions for the viscous and thermal boundary layers that incorporate wall roughness are given by Weston (1953):

$$\varphi_{vr} = d\varphi_v, \tag{17}$$

and

$$\varphi_{tr} = d\varphi_t, \tag{18}$$

where

$$d = \frac{2A}{rP}, \tag{19}$$

and d is the parameter in the nonlinear fitting of the model to the data that sets the scaling of viscous and thermal losses, P is the perimeter, and A is the cross-sectional area. P is not known and so d becomes a scaling factor that accounts for wall surface roughness, the boundary layer thickness (viscous and thermal) varying with the reciprocal of d. Keefe and Simmons (2003) included such a wall surface roughness factor in modeling calibration tube responses used to determine the acoustic output impedance of a sound source.

Values used for each of the constants (at 30 °C) were:

$$c = 349.5\,\mathrm{m/s},$$

$$\rho = 1.165\,\mathrm{kg/m^3},$$

$$\eta = 1.886 \times 10^{-5}\,\mathrm{kg/(m{\cdot}s)},$$

$$C_p = 1.005\,\mathrm{kJ/(kg{\cdot}K)},$$

$$K_t = 0.0264 \times 10^{-3}\,\mathrm{kJ/(m{\cdot}s{\cdot}K)},$$

and δ=1.4.

The input impedance of the middle ear and cochlea is given by:

$$Z_{\mathrm{me}} = \frac{1}{Y_{\mathrm{cav}}} + \frac{1}{Y_m} + Z_c, \tag{20}$$

where Y_{cav} is the admittance of the middle ear cavities, Y_m is the admittance of the five oscillators, and Z_c is the impedance of the cochlea. The admittance of the middle ear cavities, the antrum (a) and tympanum (t), is given by:

$$Y_{\mathrm{cav}} = \frac{1}{R_a + X_{C_a} + X_{M_a}} + \frac{1}{X_{C_t}}, \tag{21}$$

where R_a is the resistance of the antrum, X_{C_a} is the compliant reactance of the antrum, X_{M_a} is the mass reactance of the antrum, and X_{C_t} is the compliant reactance of the tympanum. From Kringlebotn (1988): R_a=6×10^6 kg/(s·m^4) and $X_{M_a} = i2\pi \times M_a f$, where f is frequency and M_a=10^2 kg/m^4. The compliant reactance terms were modified to match the low frequency middle ear reactance data, with a 10:1 ratio maintained between the antrum and tympanum (Kringlebotn 1988). The compliant reactance of the antrum is given by:

$$X_{C_a} = -\frac{i\rho c^2}{wV_a}, \tag{22}$$

where V_a is the volume of the antrum.

The admittance of the five oscillators is given by:

$$Y_m = \Sigma Y_i, \tag{23}$$

where

$$Y_i = \frac{1}{Z_i}, \tag{24}$$

and

$$Z_i = e_i R_m + p_i X_k + X_m. \tag{25}$$

e_i is the parameter in the nonlinear fitting of the model to the data that sets the resistance for the ith oscillator. p_i is a parameter for the ith oscillator that is determined based on local maxima in the phase data (local resonances of the middle ear). p_i is not a parameter that is free to vary in the fitting algorithm. X_k and X_m are given by:

$$X_k = \frac{-ik}{(2\pi f)}, \tag{26}$$

and

$$X_m = i2\pi f M, \tag{27}$$

R_m=10^7 kg/(s·m^4) (unless otherwise stated), k=6π×10^{10} kg/(s^2·m^4), and $M = \frac{5}{2\pi} \times 10^4$ kg/m^4. The values for k and M were derived from impedance magnitude values at 200 and 6,000 Hz, respectively, from the data of Figure 6B of O'Connor and Puria (2008).

For the cochlea, the impedance is given by:

$$Z_c = gR_c + X_c, \tag{28}$$

where g is the parameter in the nonlinear fitting of the model to the data that sets the resistance for the cochlea, R_c=10^7 kg/(s·m^4), and

$$X_c = \frac{-ik_c}{(2\pi f)}, \tag{29}$$

with k_c=10^{11} kg/(s^2·m^4) (Kringlebotn 1988).

This type of model captures well the acoustic input impedance of the middle ear. The circuit elements for the middle ear cavities and cochlea are from Kringlebotn (1988). A bank of resonant filters has been used previously by Zwislocki (1970) to represent the input impedance of the middle ear, in his mechanical coupler.

A nonlinear least squares fit was used to fit the model to the data. The nonlinear least squares fit uses the trust region reflective method. This method minimizes a smooth nonlinear function by iterations that follow piecewise linear paths (each part is linear but the overall function is nonlinear; Coleman and Li

1994). An optimal solution requires that the initial values for the free parameters be close to the final solution. Local solutions are evident when the final values vary with the choice of initial values. To avoid local solutions and find the optimal or global solution, the fitting process continued until initial and final values for each of the parameters differed by no more than 5 %.

The fitting process consisted of three steps, middle ear resistance parameters found in the first step, ear canal and cochlear parameters found in the second step, and the scaling of viscothermal losses found in the third step. The process looped or repeated until, as described in the previous paragraph, initial and final values for each of the parameters differed by no more than 5 %. This approach restricted the number of parameters free to vary at each step to five, three, and one, respectively. With nine free parameters in total, this approach was used to avoid the local solutions which can arise with a large number of free parameters.

The model was fit to the data over the frequency range 1,500–6,000 Hz where the ear canal behaves acoustically like a transmission line, excluding frequencies below 1,500 Hz where the ear canal acts like a compliant reactance and so confounds the value derived for ear canal length (and radius).

The parameters that were free to vary were a, b, d, e_i, and g, with a being the parameter that sets the final value of the radius of the ear canal, b being the parameter that sets the final value of the length of the ear canal, e_i representing the five parameters that set the final value of resistance for each of the five oscillators, g being the parameter that sets the final value of the resistance in the cochlea, and d being the parameter that sets the final value of the viscous and thermal losses.

RESULTS

Figure 2 shows the acoustic input impedance magnitude and phase spectrum for each ear and the model fit to the data for each ear (n=6). In all cases, the acoustic input impedance of the ear has a low frequency magnitude slope of −6 dB/octave and a starting phase that is near minus one quarter of a cycle, consistent with a stiffness-controlled system. As frequency increases, the influence of the middle ear becomes apparent with the magnitude slope changing and fine-structure becoming evident while the phase becomes less negative. Resonances in the middle ear, when evident, present as local minima in the magnitude response and local maxima in the phase response. Damping influences how prominent the middle ear resonances are. At around 1,500 Hz, the magnitude response starts to show evidence of the delay line property of the ear canal, transitioning to a pronounced notch at the one quarter wavelength standing wave frequency. The corresponding phase undergoes a rapid change from a negative to a positive phase, with zero phase corresponding to the one-quarter wavelength standing wave frequency resonance. The depth of the magnitude notch is a function of the impedance mismatch between the ear canal and the middle ear at the eardrum, and ear canal losses. The magnitude notch arises from the addition of an incident and a reflected wave at the microphone that are out-of-phase, the reflection occurring at the eardrum.

The data in Figure 2 shows a wide variation in acoustic input impedance magnitude and phase, from an ear with many noticeable middle ear resonances (panels f1 and f2) to an ear where the middle ear is more damped (panels a1 and a2). In all cases, the model provides a good fit to the data, while not necessarily matching every middle ear resonance (most obvious at peaks in the data phase). From the model fit to the data, the final value for the radius for all six ears was found to be less than the initial value. The initial value for the radius, the low frequency radius estimate, is an overestimate of the actual radius and so the final value is expected to be less than this value. The final value for the length of the ear canal was found in five of the six ears to exceed the SWF length, suggesting that the input impedance of the middle ear was mass-controlled at the SWF for these ears. The final value for the cochlear resistance was found to range from 1.0×10^7kg/(s·m^4) to 4.2×10^7kg/(s·m^4), the initial value in all cases being 10^7kg/(s·m^4). Considering the individual subject data and model fit to the data:

1. For Figure 2A, the radius and length of the ear canal generated by the model were 0.0039 and 0.0197 m, the initial values being 0.0047 (low-frequency estimate, see Eq. 6) and 0.0199 m (SWF value). The final value for ear canal length is almost the same as the SWF length, suggesting that for this ear the input impedance of the middle ear is resistive at the SWF. The cochlear resistance found by the model was 4.2×10^7kg/(s·m^4). Viscous and thermal boundary layers were found by the model to be about four times larger than that predicted for a smooth, rigid-walled tube.
2. For Figure 2B, the radius and length of the ear canal generated by the model were 0.0030 and 0.0191 m, the initial values being 0.0044 and 0.0173 m (SWF value). The cochlear resistance found by the model was 3.3×10^7kg/(s·m^4). Viscous and thermal boundary layers were found by the model to be five times larger than that predicted for a smooth, rigid-walled tube.

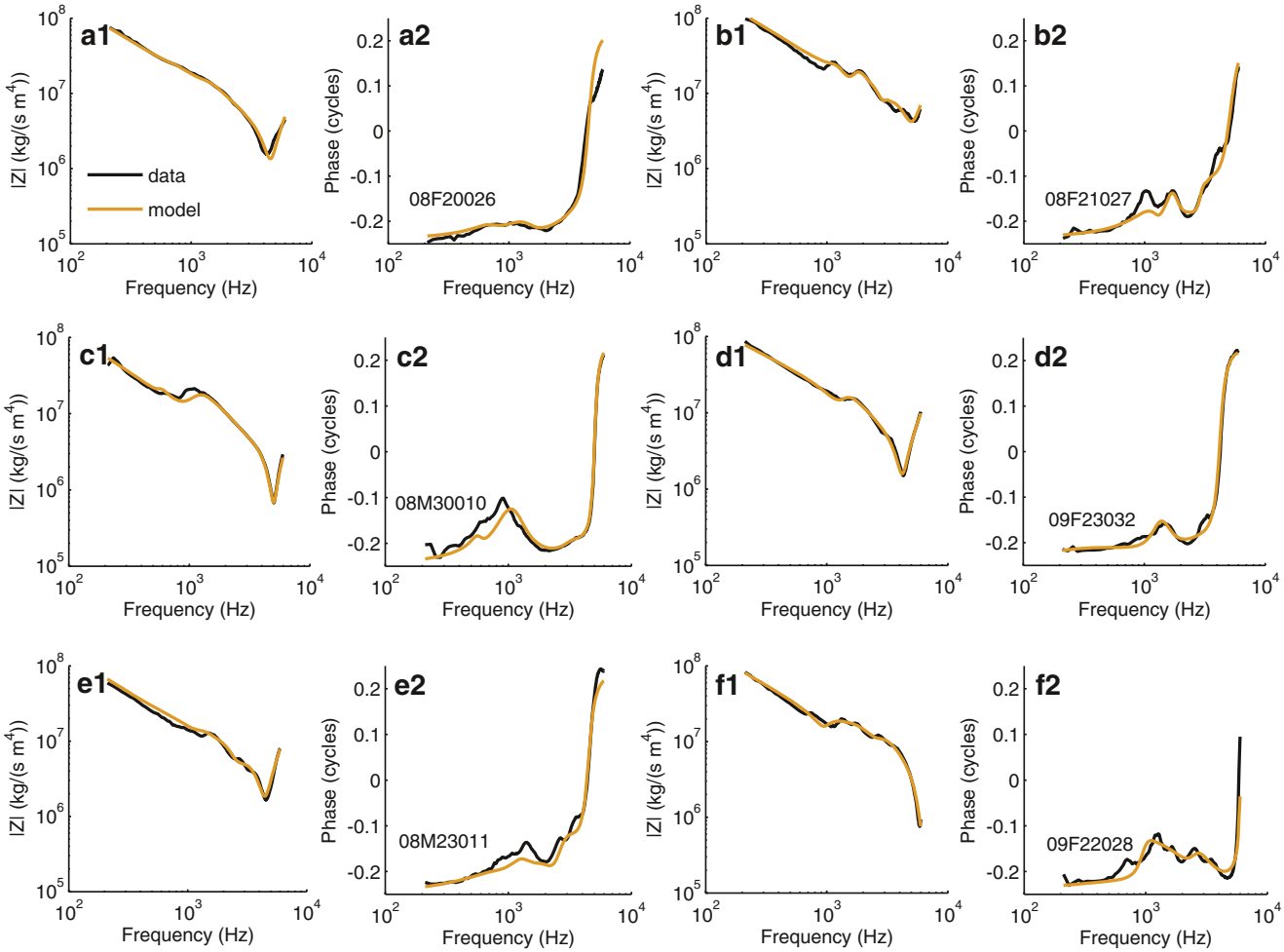

FIG. 2. Acoustic input impedance magnitude and phase data and the model fit to the data for six ears. In all cases, the model provides a good fit to the data.

3. For Figure 2C, the radius and length of the ear canal generated by the model were 0.0042 and 0.0187 m, the initial values being 0.0063 and 0.0173 m (SWF value), respectively. The cochlear resistance found by the model fit to data was 1.4×10^7kg/(s·m^4). Viscous and thermal boundary layers were found by the model to be one third the size of that predicted for a smooth, rigid-walled tube.
4. For Figure 2D, the radius and length of the ear canal generated by the model were 0.0034 and 0.0221 m, the initial values being 0.0044 and 0.0204 m (SWF value) respectively. The cochlear resistance found by the model fit to data was 2.0×10^7kg/(s·m^4). Viscous and thermal boundary layers were found by the model to be about the same size as that predicted for a smooth, rigid-walled tube.
5. For Figure 2E, the radius and length of the ear canal generated by the model were 0.0036 and 0.0223 m, the initial values being 0.0054 and 0.0197 m (SWF value) respectively. The cochlear resistance found by the model fit to data was 1.7×10^7kg/(s·m^4). Viscous and thermal boundary layers were found by the model to be about the same size as that predicted for a smooth, rigid-walled tube.
6. For Figure 2F, the radius and length of the ear canal generated by the model were 0.0037 and 0.0157 m, the initial values being 0.0054 and 0.0149 m (SWF value), respectively. The cochlear resistance found by the model fit to data was 1.0×10^7kg/(s·m^4). Viscous and thermal boundary layers were found by the model to be one third the size of that predicted for a smooth, rigid-walled tube.

Figure 3 shows the rectangular co-ordinates, input resistance, and input reactance spectra, for the middle ear and cochlea. The three responses in each panel are (1) the model middle ear response from the model fit to data; (2) the data with the model-derived ear canal removed, i.e.,

$$Z_{me} = \frac{Z_{in}Z_0 - iZ_0Z_0\tan(-il)}{Z_0 - iZ_{in}\tan(-il)}, \tag{30}$$

where Z_{in} is the acoustic input impedance of the ear data (see Eq. 1); and (3) the input resistance and input reactance spectra from Kringlebotn's model (for comparison purposes). The agreement between (1) and (2) is posited as a test of the model of the input impedance of the middle ear and cochlea, on the basis that the ear canal is well described by a uniform lossy transmission line over the frequency range considered in this study. It is notable in Figure 3 that the resistance data shows no consistent frequency dependence across subjects. The reactance data shows the general trend of being stiffness-controlled below 1 kHz and mass-controlled above 4 kHz, with multiple resonances between 1 and 4 kHz. The model does a good job of matching the overall magnitude of the resistance without capturing all of the variation. The reactance is well described by the model in all cases. Note that the initial value for R was 10^5 kg/(s·m^4) for Figure 3A and 10^6 kg/(s·m^4) for Figure 3C, being otherwise with 10^7 kg/(s·m^4) . The volume of the antrum in the model used to fit the data was respectively 0.7 cm^3 (Fig. 3A), 1.2 cm^3 (Fig. 3B), 16 cm^3 (Fig. 3C), 4 cm^3 (Fig. 3D), 10.5 cm^3 (Fig. 3E), and 2.7 cm^3 (Fig. 3F).

Figure 4 shows the results of Figure 3 recast in terms of magnitude and phase rather than resistance and reactance. In Figure 4, the normalized input admittance of the data (with the model-derived ear canal removed), and the model fit to this data, are presented. The input admittance is normalized by the admittance of the ear canal at the eardrum. A normalized input admittance value of 10° corresponds to a perfect impedance match at the eardrum between the ear canal and middle ear. In all cases, a high-pass or band-pass magnitude spectrum is evident, with the phase showing the middle ear to be stiffness-controlled at low frequencies and mass-controlled at high frequencies. There is good agreement between the model and the data. In most cases, the optimal impedance match is about −10 dB.

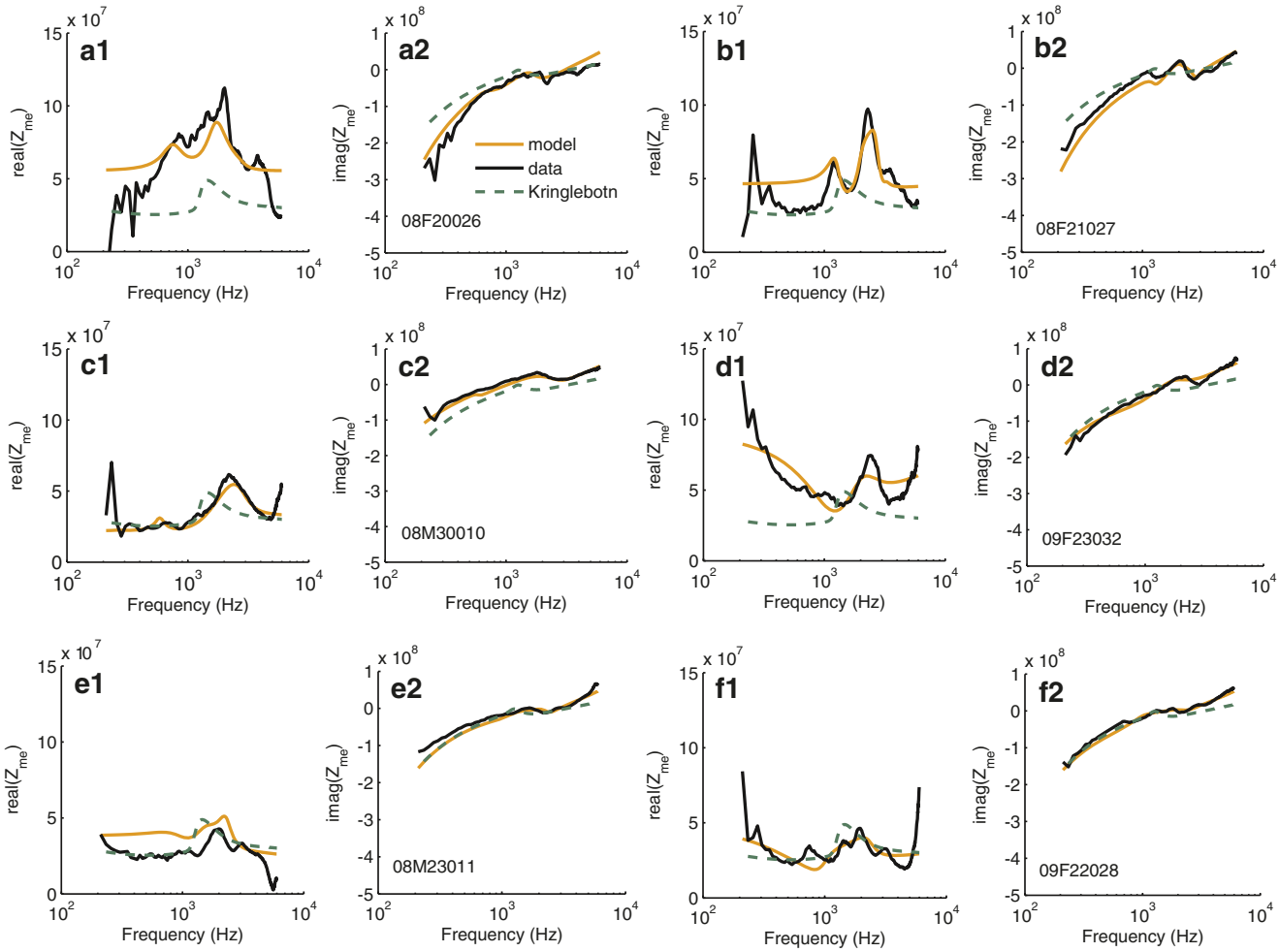

FIG. 3. Input resistance and input reactance spectra for the middle ear and cochlea. The three responses in each panel are (1) the model middle ear response from the model fit to data, (2) the data with the model-derived ear canal removed, and (3) from Kringlebotn's model of the input impedance of the middle ear and cochlea. The resistance data show no consistent frequency dependence across subjects. The reactance data show the general trend of being stiffness-controlled below 1 kHz and mass-controlled above 4 kHz, with multiple resonances between 1 and 4 kHz.

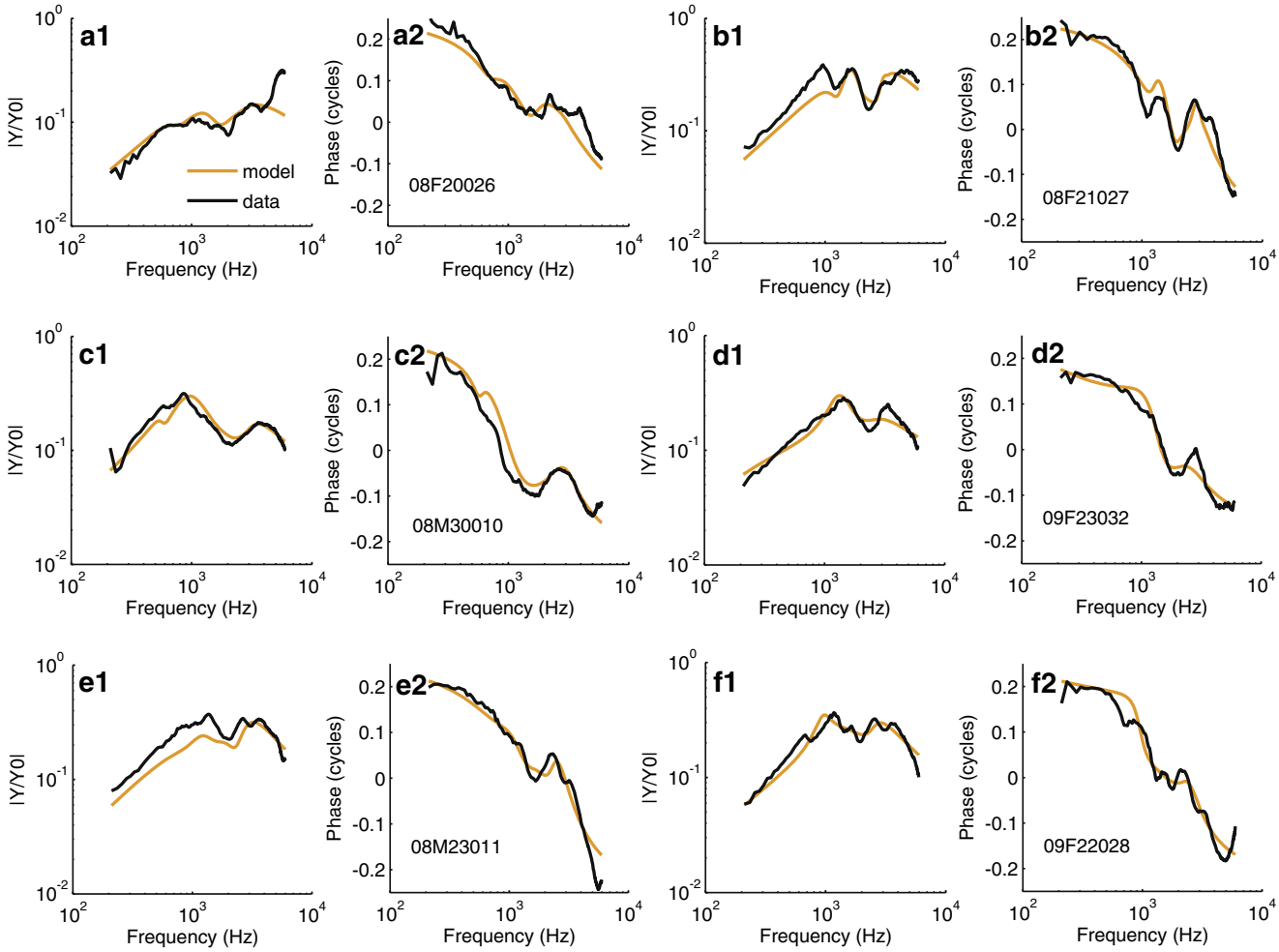

FIG. 4. The normalized input admittance, magnitude and phase, of the data with the model-derived ear canal removed, and the model fit to this data. The input admittance is normalized by the admittance of the ear canal at the eardrum. There is good agreement between the model and the data.

Figure 5 shows the cochlear input impedance magnitude and phase obtained from the model fit to the data for the six ears, as well as the average response. The magnitude of the average response is similar to that reported by Aibara et al. (2001) from a study on temporal bones, but with a greater compliant reactance contribution (at low frequencies, the phase is more negative and the magnitude decreases as frequency increases). This suggests either that the value for k_c (from Kringlebotn (1988)) used for the cochlea in the model is too large or that postmortem changes reduce cochlear stiffness.

DISCUSSION

Sound pressure measurements in the ear canal using an acoustically calibrated sound source provide for the derivation of the acoustic input impedance of the ear, providing a window into the acoustico-mechanical function of the ear. This study investigated the respective contributions of the ear canal, the middle ear, and the cochlea to the acoustic input impedance of the ear by modeling the ear as a one-dimensional lossy transmission line terminated by a distributed load impedance. Values for ear canal radius, ear canal length, and resistance that produces transmission losses, were derived from the model fit to data.

The ear canal contributes significantly to the acoustic input impedance of the ear. It is thought to be well described by a uniform cylinder or tube with rigid walls up to about 6 kHz (Stinson 1985). This would be especially true for the bony portion of the ear canal, the region of the ear canal examined in this study. The radius of the ear canal derived from the model fit to acoustic input impedance data ranged from 3.0 to 4.2 mm, consistent with that found by other investigators using physical methods of measurement (Bekesy 1960; Voss et al. 2008). Of course, the radius is location dependent, the ear canal radius increasing with distance from the eardrum (Stinson 1990; Voss et al. 2008). Derivation of the radius of the

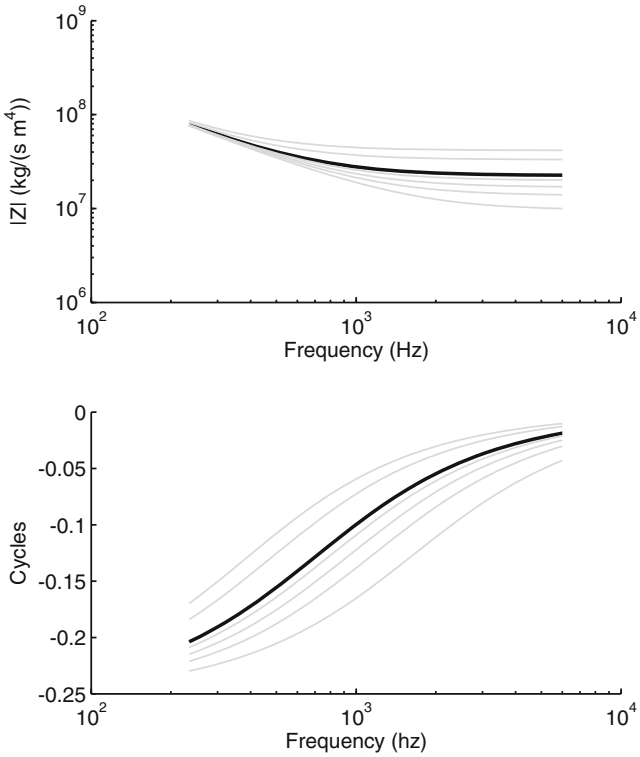

FIG. 5. The input impedance of the cochlea from the model fit to the data for each of the six ears and the average of this model impedance. The average response suggests a reactive compliance below 1 kHz but predominantly a resistive cochlear input impedance.

ear canal has application to quantifying the impedance mismatch between the ear canal and the middle ear at the eardrum,[2] i.e., in calculating reflectance. The length of the ear canal and the length calculated from the one quarter wavelength SWF differ because the ear canal termination (the middle ear) is non-rigid. Chan and Geisler (1990) found the SWF length to always be less than the physical length to the umbo (14 ears), the difference ranging from ≈1 to 6 mm, with a mean of 3 mm. In this study, the difference ranged from –0.2 to 2.6 mm, the positive difference for five of the six ears being consistent with the input impedance of the middle ear being mass-controlled at the SWF. The Chan and Geisler (1990) study used open ear canals and so the SWF would be lower than for this study and would therefore be less likely to correspond to a frequency where the middle ear was mass-controlled.

Ear canal viscothermal losses were calculated in this study, with allowance made for the ear canal to not act as a smooth, rigid-walled surface. Two studies that have explicitly examined viscothermal losses in the ear canal examined reflectance as a function of ear canal measurement position (Farmer-Fedor and Rabbitt 2002; Voss et al. 2008). Both studies found little or no positional dependence for the derivation of reflectance magnitude, arguing against significant viscothermal losses in the ear canal. In this study, viscothermal losses were calculated to have a boundary layer that ranged from one third the size of that predicted by Kirchhoff's theory to five times that predicted by Kirchhoff's theory. Inspection of Figure 2, magnitude and phase responses, around the SWF, suggests an identifiable impact of viscothermal losses; the slope of the magnitude above the SWF, and the slope of the phase around resonance, is observed to decrease with increasing frequency.

A boundary layer less than that calculated for a smooth, rigid-walled surface is not permitted based on Kirchhoff's theory. A boundary layer greater than that predicted by Kirchhoff's theory argues for wall surface roughness to increase the size of the boundary layer. Constraining the analysis to not produce a boundary layer less than that for a smooth rigid-walled surface in deriving the best fit to the data is probably warranted.

The middle ear (and cochlea) was examined in terms of resistance and reactance. Resistance showed no specific frequency dependence. The average value for resistance for three of the six subjects was similar to that of the middle ear model (based on 20 cadaver ears) of Kringlebotn (1988), about $4\times10^7 \mathrm{kg}/(\mathrm{s}\cdot\mathrm{m}^4)$. For the other three ears, the average resistance was greater than that predicted by Kringlebotn's model,

[2] The impedance of the ear canal at the eardrum is a function of the radius of the ear canal.

illustrating simply that Kringlebotn's model is based on averaged data and circuit elements would need to be modified to account for individual subject variation. In all cases, the cochlear resistance was not the major source of damping suggested by Zwislocki (1962), the middle ear contributing significant damping to the acoustic input impedance of the ear. The reactance shows the general trend of being stiffness-controlled at low frequencies and mass-controlled at high frequencies, with multiple resonances between 1 and 4 kHz. The volume of the antrum in the model that provided the observed match to the low frequency reactance ranged from 0.7 to 16 cm^3, values above 2 cm^3 being commensurate with that reported by Zwislocki (1962). The volume of the tympanum was maintained at a 1:10 ratio with the antrum (Kringlebotn 1988). The two lowest antrum volumes indicate another source of stiffness in the middle ear, these volumes presumably being too small to be physiological. The reactance from Kringlebotn's middle ear model (a variant of Zwislocki's 1962 model) does not capture the variation in low frequency stiffness across subjects, but does have the same trend of being stiffness-controlled at low frequencies; it does not show a mass-controlled system at high frequencies. Kringlebotn's model used a value for tympanum volume of 5.2 cm^3. Presumably Kringlebotn's model could provide a better fit to individual data with subject-specific changes to the values of the model elements.

The frequency response of the normalized input admittance of the middle ear is bandpass, similar to that reported by Rabinowitz (1981) up to 4 kHz, with the middle ear becoming mass-controlled above 4 kHz. The frequency response differs from the more narrowly tuned response reported by O'Connor and Puria (2008), suggesting that postmortem changes may simplify the tuning properties of the middle ear although Voss et al. (2000) reported an input impedance magnitude and phase from temporal bones more consistent with Figure 4. The impedance match provided by the middle ear to the ear canal at the eardrum was found to be, at best, a 10 dB reduction with respect to a perfect impedance match. The model of Kringlebotn (1988) suggests a similar value, the model based on measurements in temporal bones.

This study extends the work of Kringlebotn (1988) to investigate the acoustico-mechanics of the ear in healthy human ears. It quantifies the contributions of the ear canal, middle ear, and cochlea, to the total damping, and furnishes values for ear canal radius and length based on sound pressure measurements in the ear canal, in individual ears. The technique to acoustically calibrate a sound source in terms of its Thevenin source pressure and source impedance, developed by Allen (1986) and Keefe et al. (1992), provided the means to generate acoustic input impedance data from sound pressure measurements in the ear canal. Future work would include substituting other models of the middle ear for the model used in this study to investigate structure–function relationships of the middle ear further.

ACKNOWLEDGMENTS

Robert Withnell is indebted to the School of Mechanical Engineering at The University of Western Australia for generously hosting his sabbatical and for the award of a Gledden Senior Research Fellowship that provided the impetus for this work. Doug Keefe, Mead Killion, and one anonymous reviewer, provided valuable feedback and advice on earlier versions of this paper. Portions of this paper were presented at the Mechanics of Hearing 2011 conference in Williamstown, MA, USA and the American Auditory Society conference in Scottsdale, AZ, USA.

REFERENCES

AIBARA R, WELSH J, PURIA S, GOODE R (2001) Human middle-ear sound transfer function and cochlear input impedance. Hear Res 152:100–109

ALLEN J (1986) Measurement of eardrum acoustic impedance. In: Allen JB, Hall JL, Hubbard A, Neely ST, Tubis A (eds) Peripheral auditory mechanisms. Springer, New York, pp 44–51

BEKESY G (1960) Experiments in hearing. McGraw Hill, New York

BENADE A (1968) On the propagation of sound waves in a cylindrical conduit. J Acoust Soc Am 44:616–623

CHAN J, GEISLER C (1990) Estimation of eardrum acoustic pressure and of ear canal length from remote points in the canal. J Acoust Soc Am 87:1237–1247

COLEMAN T, LI Y (1994) On the convergence of interior-reflective Newton methods for nonlinear minimization subject to bounds. Math Program 67:189–224

FARMER-FEDOR B, RABBITT R (2002) Acoustic intensity, impedance and reflection coefficient in the human ear canal. J Acoust Soc Am 112:600–620

HENRY P (1931) The tube effect in sound-velocity measurements. Proc Phys Soc 43:340–362

HUANG G, ROSOWSKI J, PURIA S, PEAKE W (2000) Tests of some common assumptions of ear-canal acoustics in cats. J Acoust Soc Am 108:1147–1161

KAYE G, SHERRATT G (1933) The velocity of sound in gases in tubes. Proc R Soc A 141:123–143

KEEFE D, SIMMONS J (2003) Energy transmittance predicts conductive hearing loss in older children and adults. J Acoust Soc Am 114:3217–3238

KEEFE D, LING R, BULEN J (1992) Method to measure acoustic impedance and reflection coefficient. J Acoust Soc Am 91:470–485

KRINGLEBOTN M (1994) Acoustic impedance in the human ear canal. Scandanavian Audiology 23:65–71

KRINGLEBOTN M (1988) Network model for the human middle ear. Scand Audiol 17:75–85

LYNCH T, PEAKE W, ROSOWSKI J (1994) Measurements of the acoustic input impedance of cat ears: 10 hz to 20 khz. J Acoust Soc Am 96:2184–2209

MARGOLIS R, SALY G, KEEFE D (1999) Wideband reflectance tympanometry in normal adults. J Acoust Soc Am 106:265–280

MOLLER A (1961) Network model of the middle ear. J Acoust Soc Am 33:168–176

MOLLER A (1965) An experimental study of the acoustic impedance of the middle ear and its transmission properties. Acta Oto-Laryngologica 60:129–149

O'CONNOR K, PURIA S (2008) Middle-ear circuit model parameters based on a population of human ears. J Acoust Soc Am 123:197–211

PARENT P, ALLEN J (2007) Wave model of the cat tympanic membrane. J Acoust Soc Am 122:918–931

RABINOWITZ W (1981) Measurement of the acoustic input immittance of the human ear. J Acoust Soc Am 70:1025–1035

SHIELDS F, LEE K, WILEY W (1965) Numerical solution for sound velocity and absorption in cylindrical tubes. J Acoust Soc Am 37:724–729

STINSON M (1985) The spatial distribution of sound pressure within scaled replicas of the human ear canal. J Acoust Soc Am 78:1596–1602

STINSON M (1990) Revision of estimates of acoustic energy reflectance at the human eardrum. J Acoust Soc Am 88:1773–1778

VOSS S, ALLEN J (1994) Measurement of acoustic impedance and reflectance in the human ear canal. J Acoust Soc Am 95:372–384

VOSS S, ROSOWSKI J, MERCHANT S, PEAKE W (2000) Acoustic responses of the human middle ear. Hear Res 150:43–69

VOSS S, HORTON N, WOODBURY R, SHEFFIELD K (2008) Sources of variability in reflectance measurements on normal cadaver ears. Ear Hear 29:651–665

WESTON D (1953) The theory of the propagation of plane sound waves in tubes. Proc Phys Soc B 66:695–709

WITHNELL R, JENG P, WALDVOGEL K, MORGENSTEIN K, ALLEN J (2009) An in-situ calibration for hearing thresholds. J Acoust Soc Am 125:1605–1611

ZWISLOCKI J (1962) Analysis of the middle-ear function. part i: Input impedance. J Acoust Soc Am 34:1514–1523

ZWISLOCKI J (1970) An acoustic coupler for earphone calibration (Tech. Rep. No. LSC-S-7). Syracuse University